Energy-efficient dynamic point selection and scheduling method for intra-cell CoMP in LTE-A

Olli Apilo · Mika Lasanen · Aarne Mämmelä

Abstract In this paper, we propose a novel dynamic point selection (DPS) and user scheduling method for improving the energy efficiency in distributed antenna systems without cell edge spectral efficiency degradation. When DPS is used, each user is served by a single transmission point that can be dynamically switched. The proposed method decreases the power consumption by switching off inactive radio frequency (RF) chains and additionally reduces the interference by a static inter-cell agreement on which transmission points are simultaneously active. The performance of the method is evaluated by computer simulations in a system that accurately models the LTE-Advanced (LTE-A) intra-cell coordinated multi-point (CoMP) scenario 4. Based on the performance simulations, the proposed method achieves a significant energy efficiency gain over closed-loop spatial multiplexing applied on localized or distributed transmitting antennas. In general, the proposed method performs well when the load-independent RF power consumption is high in the active mode and low in the sleep mode. When the proportion of the load-independent RF power consumption to the total load-independent power consumption exceeds a certain limit, which is 22 % in the case of 10 users in the 3-sector layout, the proposed method brings always energy efficiency gain even when RF chain micro sleeping cannot be implemented. The usability of the method is not dependent on the traffic load. The same approach can be applied to any distributed antenna system.

O. Apilo · M. Lasanen · A. Mämmelä
VTT Technical Research Centre of Finland, Oulu, Finland
E-mail: olli.apilo@vtt.fi

M. Lasanen
E-mail: mika.lasanen@vtt.fi

A. Mämmelä
E-mail: aarne.mammela@vtt.fi

1 Introduction

Energy consumption in cellular networks is expected to increase with the increasing wireless traffic. Currently there are over 4 million base stations globally each consuming 25 MWh per year on average [1]. Cost of energy is becoming more and more important for telecommunications operators and thus any improvement on the energy efficiency decreases the operational expenses (OPEX). In addition to reduced OPEX, energy efficiency improvements help to reduce the CO_2 emissions from the electrical energy generation. In recent years, improving energy efficiency in cellular networks has been an active research topic ranging from component-level to network-level solutions [2].

3GPP Long Term Evolution (LTE) and LTE-Advanced (LTE-A) were primarily designed for fulfilling the International Mobile Telecommunications-Advanced (IMT-A) requirements [3] for 4G radio interface [4]. Energy efficiency was not included to the requirements and thus it has not been a major concern until recently. The potential energy efficiency improvements for LTE have been discussed in [5] where the energy saving techniques are divided into time, frequency, and space domains. The time domain techniques include different variants of discontinuous transmission (DTX) methods [6] that are based on minimizing the number of transmitted control signals when there is no payload data to be transmitted. When the enhanced DTX is used, only the synchronization and broadcast signals are mandatory and radio frequency (RF) circuits can be switched off for several milliseconds when there is no payload data to be transmitted. The frequency domain methods restrict the used bandwidth into a fraction of the available bandwidth. The energy saving is smaller when compared to time domain methods because the RF circuits remain active and only the transmission power is reduced. The space domain methods include base station sleep modes during which a low load base station is turned off and its previously served users are handed over to neighbouring cells [7]. At a smaller scale, also individual base station antennas together with their RF circuitry can be turned off to save energy.

It is well known that multiple-input multiple-output (MIMO) systems can provide significant gain in spectral efficiency when compared to single-input multiple-output (SIMO) systems [8]. However, it is not obvious whether the additional transmitting antennas bring any energy efficiency gain. This problem in the context of single user MIMO (SU-MIMO) has been studied for transmitter diversity with and without transmitter channel state information (CSI) in [9] and [10], respectively. In both cases, single-input single-output (SISO) was found to be more energy efficient when the distance between the transmitter and the receiver is short. When spatial multiplexing is enabled by multiple antennas at the receiver, it was shown in [11] that a MIMO system with two transmitting antennas in a Rayleigh fading channel is not necessarily more energy efficient than a SISO system when there is no CSI available at the transmitter. Using more than two transmitting antennas was found to be energy inefficient when compared to SISO. Similar findings have been reported in [12] for a distributed MIMO system with no CSI at the transmitter. Results

in [9–12] suggest that antenna selection at the transmitter is generally a very energy-efficient transmission strategy for SU-MIMO when the full instantaneous CSI cannot be made available for the transmitter. Also for the multi user MIMO (MU-MIMO) systems, transmission from all available antennas is not typically energy-efficient but rather the set of active transmitting antennas should be dynamically optimized [13].

Although downlink (DL) antenna selection is not explicitly supported in LTE, its distributed variant, dynamic point selection (DPS), is one of the coordinated multi-point (CoMP) methods in LTE-A. CoMP uses transmitting and receiving antennas from multiple different geographical locations to improve the cell edge user throughput [14]. When DPS is used, the transmission point (TP) serving a user equipment (UE) can be switched dynamically according to the available resources and the channel quality. DPS is enabled by configuring several CSI processes, one for each potential TP, for reporting the channel quality from UE to enhanced Node B (eNB) [15]. Four different CoMP scenarios have been defined in [16]. The focus in our work is on Scenario 4 in which low power remote radio heads (RRHs) have the same cell ID as the eNB, i.e. RRHs can be considered as remote antennas for the eNB.

In this paper, we present a novel and practical DPS and time domain UE scheduling algorithm as a solution to the problem how to improve the energy efficiency under full load in the intra-cell CoMP scenario 4 such that the cell edge spectral efficiency is not degraded. The key idea of the algorithm is to transmit from only one antenna of the cell during a subframe and switch the inactive RF circuits off for power consumption reduction. In addition, the inter-cell interference is reduced by a static inter-cell agreement on which TPs are active at a given subframe. Our method provides significant energy efficiency improvement when compared to localized or distributed SU-MIMO.

The idea of enabling very short millisecond-level micro sleep modes of the eNB hardware by DTX was first presented in [6]. The decision to enter into the micro sleep mode is done if there is no UE traffic to be served or no mandatory control signals to be transmitted. Thus, the proposed method in [6] is applicable only under low load. The minimization of the base station supply power under the target per-UE data rates is presented in [17]. The proposed algorithm solves the optimum number of transmitting antennas, the number of micro sleep mode time slots, and the number of resource elements per UE. Unlike in our work, inter-cell interference is not considered in [17] and the transmitting antennas are assumed to be localized. The idea of statically agreeing the micro sleep schedules between neighbouring cells was presented in [18]. It was shown that even under full load energy efficiency is improved when compared to the normal always-on configuration by coordinating the sleep modes orthogonally between the closest cells. Our proposal on statically agreeing which TPs are active can be seen as an extension of the idea in [18] to the scenarios with distributed antennas.

The remainder of the paper is organized as follows: The system model is described in Section 2. The research problem and the proposed DPS and scheduling method is presented in Section 3. In Section 4, we formulate the

criteria for the RRH location that maximizes the cell edge spectral efficiency. The results of the numerical simulations that compare the proposed method to localized and distributed MIMO based on closed-loop spatial multiplexing are given in Section 5. Finally, conclusions are drawn in Section 6.

Notation: We use the following notation throughout this paper: bold lowercase $\mathbf{a}$ is used to denote a column vector, bold uppercase $\mathbf{A}$ denotes a matrix whose jth column vector is given by $\mathbf{a}_j$. Non-bold letters a, A denote scalars and calligraphic letters $\mathcal{A}$ are used for sets. The magnitude of scalar a is $|a|$ and $\|\mathbf{a}\|$ denotes the l_2 norm of vector $\mathbf{a}$. The size of a set is denoted by $|\mathcal{A}|$. $\mathbf{A}^T$ and $\mathbf{A}^H$ denote the transpose and the conjugate transpose of matrix $\mathbf{A}$, respectively. The inverse of matrix $\mathbf{A}$ is written as $\mathbf{A}^{-1}$. The identity matrix is given by $\mathbf{I}$. The operators $\min\{a, b\}$ and $\max\{a, b\}$ denote the minimum and maximum of elements a and b, respectively. The expected value of random variable X is denoted by $E[X]$.

2 System Model

We consider a frequency division duplex (FDD) LTE-A DL system in a sectored cell layout with full frequency reuse, i.e. the same carrier frequency is used in each sector of each site. As recommended in [19], the cloverleaf layout is used for the 3-sector sites. For 6-sector sites, we apply the snowflake layout proposed in [20]. The cloverleaf and snowflake layouts have been shown to reach better coverage and capacity than the traditional hexagonal layouts [21]. There is no such backhaul links between sites that would allow dynamic intersite cooperation. The used layouts are shown in Fig. 1. Each site is equipped by $\Gamma \cdot N$ localized or distributed antennas, where $\Gamma \in \{3, 6\}$ is the number of sectors and N is the number of antennas per sector. Low-power RRHs have been deployed to improve the performance of cell edge UEs. When distributed antennas are used, there are $\Gamma \cdot (N - 1)$ single-antenna low-power RRHs and a Γ-antenna eNB deployed onto the site. Each RRH is connected to the eNB via a low-latency, high-capacity point-to-point fiber link. This corresponds to the 3GPP CoMP deployment scenario 4. The recommendations for simulating the performance of CoMP deployment scenario 4 given in [16] are mostly followed in our work. The sector layouts and dominant interferers in the distributed case when $N = 2$ are shown in Figs. 2 and 3 for three and six sectors, respectively. The dominant interfering sectors are numbered and the payload and interfering signals are depicted with green and dashed red arrows, respectively.

Throughout this paper we assume that users are randomly located according to the uniform distribution. According to the normal cell search procedure, UEs do not necessarily connect to the closest sector but rather to the sector from which the average received reference signal power is the highest. The RRHs are assumed to be also randomly located according to the uniform distribution. In addition, we propose a deterministic RRH placement strategy for improving the cell edge performance in Section 4.
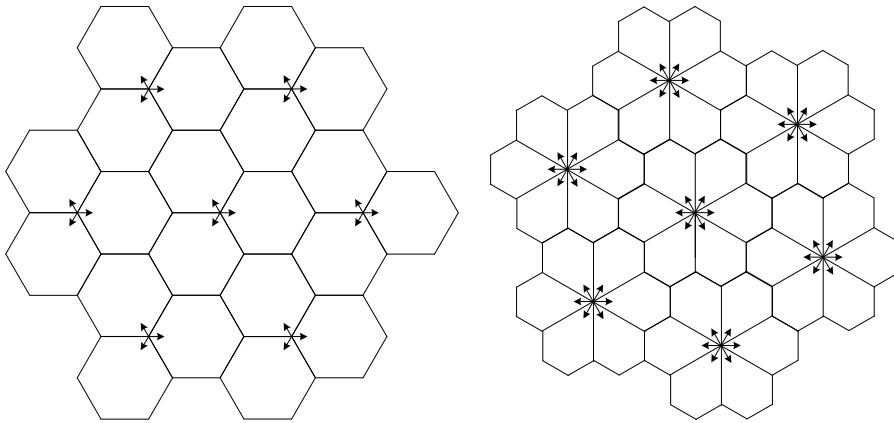
Fig. 1 The 3-sector cloverleaf (left) and 6-sector snowflake (right) cellular layouts
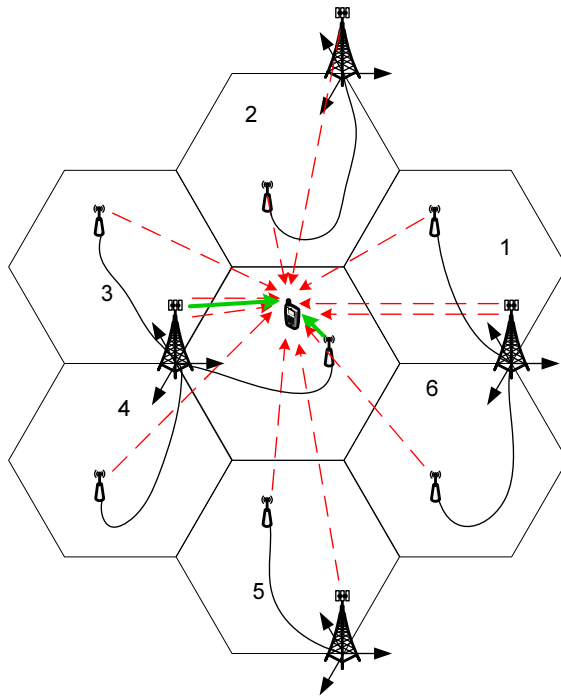
Fig. 2 Sector layout and dominant interferers for the 3 sector deployment

We assume that SU-MIMO based on closed-loop spatial multiplexing, i.e. transmission mode 4 [22], is used when no DPS is employed. This assumption is valid for systems where the peak UE spectral efficiency or cell edge spectral efficiency is maximized instead of sum spectral efficiency. For DPS, we assume that transmission mode 10, which is designed for CoMP transmission [23],

Fig. 3 Sector layout and dominant interferers for the 6 sector deployment
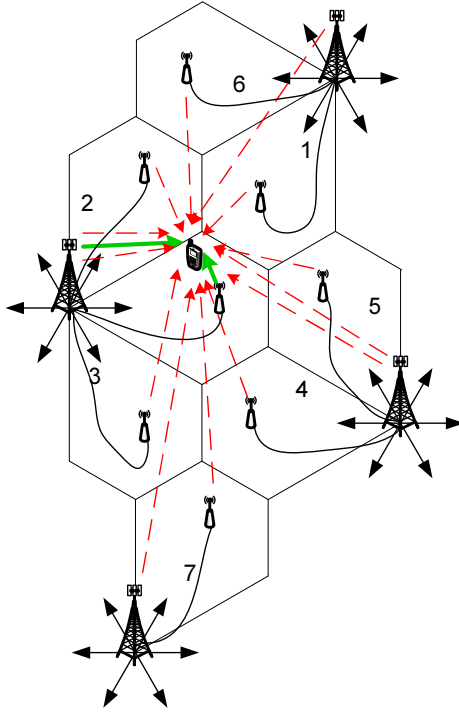
is used. The number of antennas at each UE is $M \geq N$ and the number of dominant interferers $I = 6$ and $I = 7$ for 3 and 6 sectors, respectively. The number of transmission layers $J \leq N$ equals the rank indicator (RI) that is signalled by the UE.

DL in LTE systems is based on orthogonal frequency domain multiplexing (OFDM). In order to simplify the notation, the frequency domain subcarrier indexing and the time domain OFDM symbol indexing of the resource element are omitted from the following description. The complex frequency domain received signal on the given resource element for UE k can be written as

$$\mathbf{y}^{(k)} = \mathbf{H}^{(k)}\mathbf{W}^{(k)}\mathbf{x}^{(k)} + \sum_{i=1}^{I} \mathbf{H}^{(k,i)}\mathbf{W}^{(i)}\mathbf{x}^{(i)} + \mathbf{n}^{(k)} \tag{1}$$

where $\mathbf{y}^{(k)}$ is the $M \times 1$ received signal vector, $\mathbf{H}^{(k)}$ is the $M \times N$ channel matrix, $\mathbf{W}^{(k)}$ is the $N \times J$ transmitter filtering matrix, $\mathbf{x}^{(k)}$ is the $J \times 1$ transmitted signal vector with $E[\mathbf{x}\mathbf{x}^H] = \mathbf{I}$, $\mathbf{H}^{(k,i)}$ is the channel matrix between interferer i and UE k, and $\mathbf{n}^{(k)}$ is the $M \times 1$ noise vector whose entries are i.i.d. complex Gaussian distributed with zero mean and variance σ^2. The sum term in (1) corresponds to the inter-cell interference from the I dominant interferers. The transmitter filtering matrix can be further divided into the $N \times J$ precoding

matrix $\mathbf{V}^{(k)}$ defined in [22] and the $N \times N$ diagonal power loading matrix $\mathbf{Q}$ such that $\mathbf{W}^{(k)} = \mathbf{Q}\mathbf{V}^{(k)}$. DPS can be modelled by selecting the precoding vector from $\mathbf{V} \in \left\{ [1 \ 0 \ \ldots \ 0]^T, [0 \ 1 \ \ldots \ 0]^T, \ \ldots \ [0 \ 0 \ \ldots \ 1]^T \right\}$. Power loading matrix $\mathbf{Q}$ is defined as $Q_{nn} = \sqrt{G_{\mathrm{eNB}}}$, $\forall n$ for the localized scenario. For the distributed scenario, $Q_{11} = \sqrt{2G_{\mathrm{eNB}}}, Q_{nn} = \sqrt{2G_{\mathrm{RRH}}}, n = 2, \ldots, N$ for closed-loop spatial multiplexing and $Q_{11} = \sqrt{G_{\mathrm{eNB}}}, Q_{nn} = \sqrt{G_{\mathrm{RRH}}}, n = 2, \ldots, N$ for DPS. G_{eNB} and G_{RRH} are the transmitted power gains for eNB and RRH, respectively.

The channel coefficient between transmitting antenna n and receiving antenna m is

$$H_{m,n}^{(k)} = 10^{\left(G_{\mathrm{ant}} + A(\theta_n^{(k)}, d_n^{(k)}) - \Lambda(d_n^{(k)}) + S_n^{(k)} \right)/20} \cdot F_{m,n}^{(k)} \tag{2}$$

where G_{ant} is a constant representing the sum of antenna gains and connector losses in dB, $A(\theta_n^{(k)}, d_n^{(k)})$ is the transmitting antenna directional pattern in dB as a function of the direction $\theta_n^{(k)}$ to the UE relative to the antenna boresight and the distance $d_n^{(k)}$ between the UE and the transmitting antenna, $\Lambda(d_n^{(k)})$ is the distance-dependent path loss term in dB, $S_n^{(k)}$ is the shadowing term in dB that is normally distributed with zero mean and variance σ_S^2, and $F_{m,n}^{(k)}$ is the complex multipath fading term. The antenna directional pattern is specified as [19]

$$A(\theta, d) = \begin{cases} -\min\left[-\left(A_h(\theta) + A_v(d) \right), A_m \right], & \text{for eNB} \\ 0, & \text{for RRH} \end{cases} \tag{3}$$

where the horizontal antenna pattern $A_h(\theta)$ is

$$A_h(\theta) = -\min\left[12 \left(\frac{\theta}{\theta_{\mathrm{3dB}}} \right)^2, A_m \right] \tag{4}$$

and the vertical antenna pattern $A_v(d)$ is

$$A_v(d) = -\min\left[12 \left(\frac{\tan^{-1}(h/d) - \phi_{\mathrm{tilt}}}{\phi_{\mathrm{3dB}}} \right)^2, A_{m,v} \right]. \tag{5}$$

The maximum attenuations in the horizontal and vertical direction are denoted by A_m and $A_{m,v}$, respectively. ϕ_{tilt} is the tilt angle, h is the height difference between transmitting and receiving antennas, and θ_{3dB} and ϕ_{3dB} are the 3 dB beamwidths in horizontal and vertical directions, respectively. All angles in (4) and (5) are given in degrees. The path loss is modelled as $\Lambda(d) = \kappa + 10\alpha \log_{10}(d)$ where κ is a constant parameter depending on the propagation scenario and α is the path loss exponent. Multipath fading is modelled using a frequency-selective tapped delay line model with Rayleigh fading taps such that the mean power gain of $F_{m,n}^{(k)}$ is normalized to unity. The number of taps and their power-delay profile are modelled according to the Urban Macro non-line-of-sight (NLoS) and Urban Micro NLoS clustered delay line models [19] for eNB-UE and RRH-UE links, respectively. It is assumed that the channel

Table 1 Mapping of effective SNR to CQI indices

Effective SNR in dB exceeds	CQI index	Efficiency
$-\infty$	0	out of range
-6.934	1	0.1523
-5.147	2	0.2344
-3.180	3	0.3770
-1.254	4	0.6016
0.761	5	0.8770
2.700	6	1.1758
4.697	7	1.4766
6.528	8	1.9141
8.576	9	2.4063
10.37	10	2.7305
12.30	11	3.3223
14.18	12	3.9023
15.89	13	4.5234
17.82	14	5.1152
19.83	15	5.5547

is block fading in the time domain with channel block duration of 10 ms, i.e. one LTE frame.

In transmission mode 4, UE feeds back the channel quality indicator (CQI), RI, and precoding matrix indicator (PMI) to eNB by uplink (UL) signalling [23]. In transmission mode 10, only CQI reporting is configured for DPS. CQI is used for selecting the suitable modulation and coding scheme (MCS) for DL transmission, RI is used for selecting the number of transmission layers, and PMI is used for selecting the precoding matrix from the pre-defined codebook. We assume that both CQI and PMI are reported per physical resource block (PRB) to enable frequency selective scheduling of UEs. It is also assumed that indicators are available at eNB for scheduling and link adaptation at the beginning of each 10 ms channel block. All the indicators are functions of the received post-processing signal-to-interference-plus-noise ratio (SINR) that is calculated from channel state information reference signals (CSI-RSs) and interference measurement resources (IMRs) [15]. We use the procedure for mapping between the post-processing SINR and PMI, RI, and CQI from [24]. Since CSI-RS is mapped to only one resource element per PRB in the frequency domain [25], the effective signal-to-noise ratio (SNR) for a PRB is set to equal the post-processing SINR for a PRB. The effective SNR values are then mapped into CQI indices according to Table 1 [26]. The details of deriving the effective SNR limits shown in Table 1 are described in [27].

Assuming detection by linear filtering, the post-processing received signal is given by $\mathbf{r}^{(k)} = (\mathbf{G}^{(k)})^H \mathbf{y}^{(k)}$, where $(\mathbf{G}^{(k)})^H$ is $J \times M$ receive filtering matrix. The post-processing SINR for layer j of UE k $\gamma_j^{(k)}$ can be given as

$$\gamma_j^{(k)} = \frac{\left| (\mathbf{g}_j^{(k)})^H \mathbf{H}^{(k)} \mathbf{w}_j^{(k)} \right|^2}{I_{\text{self}} + I_{\text{out}} + \sigma^2 \left\| \mathbf{g}_j^{(k)} \right\|^2} \tag{6}$$

where

$$I_{\text{self}} = \sum_{a \neq j} \left| (\mathbf{g}_j^{(k)})^H \mathbf{H}^{(k)} \mathbf{w}_a^{(k)} \right|^2 \tag{7}$$

is the self-interference between layers of the UE and

$$I_{\text{out}} = \sum_{i=1}^{I} \left\| (\mathbf{g}_j^{(k)})^H \mathbf{H}^{(k,i)} \mathbf{W}^{(i)} \right\|^2 \tag{8}$$

is the out-of-cell interference. Following the guidelines given in [16], we assume that the detection is done by linear minimum mean square error (MMSE) filtering such that

$$(\mathbf{G}^{(k)})^H = \left(\tilde{\mathbf{H}}^{(k)} \right)^H \left(\tilde{\mathbf{H}}^{(k)} \left(\tilde{\mathbf{H}}^{(k)} \right)^H + \mathbf{Z} \right)^{-1} \tag{9}$$

where $\tilde{\mathbf{H}}^{(k)} = \mathbf{H}^{(k)} \mathbf{W}^{(k)}$ and $\mathbf{Z}$ is $M \times M$ diagonal matrix with diagonal elements

$$Z_{m,m} = \sigma^2 + \sum_{i=1}^{I} \sum_{j=1}^{J} \left| \tilde{H}_{m,j}^{(k,i)} \right|^2 . \tag{10}$$

The effect of imperfect channel estimation would be similar to all considered methods. Thus for simplicity, it is assumed that the receiver has the perfect channel knowledge.

In addition to the MCS selection, the reported CQI values are also used for scheduling of UEs. We apply a simple frequency-domain scheduling algorithm based on the resource fair principle [28] such that the same number of PRBs is allocated for each UE. The objective is to maximize the throughput of the considered UE by selecting from the set of available PRBs those with the highest reported CQI values. The UEs are scheduled in the descending order of the average potential throughput calculated over the set of available PRBs. In the time domain, all UEs are scheduled for each subframe when no DPS is applied. The time domain scheduling for DPS is presented in Section 3. In this paper, we assume that the number of scheduled UEs never exceeds the maximum number of DL control channel elements, i.e. there is no need for additional round-robin mechanism to guarantee the resource fair principle.

To improve the energy efficiency in low load situations, we assume that a slightly modified version of the enhanced cell DTX scheme [6] is used in the network. In case of no user traffic, only the synchronization, broadcast, cell-specific reference signals, and CSI-RSs have to be transmitted in subframes 0 and 5 and there is no transmission during the 8 other subframes. Thus, enhanced DTX enables very short sleep modes in the order of milliseconds, during which some RF components can be switched off. The model for the consumed power P_c in sector c is derived by combining the OPERA-Net base station power consumption model [29] with the sleep mode modelling from [30]:

$$P_c = P_P + \sum_{n=1}^{N} \left(s_n a P_{R,n} + (1 - s_n) \left(P_{R,n} + P_{\text{PA}}(P_{\text{in},n}) \right) \right) \tag{11}$$

where P_P is the power consumption of the digital baseband processing, $s_n \in \{0, 1\}$ is the sleep mode state indicator, $P_{R,n}$ is the load-independent power consumption of the RF processing, and $P_{\mathrm{PA}}(P_{\mathrm{in},n})$ is the load-dependent power consumption of the RF processing that is a function of the RF input power to the power amplifier (PA) $P_{\mathrm{in},n}$. The parameter a, $0 \leq a \leq 1$ indicates the fraction of the load-independent RF power consumption while in sleep mode. RF input power at sample instant t to antenna n can be given as

$$P_{\mathrm{in},n}(t) = \frac{1}{\sqrt{N_{\mathrm{FFT}}}} \left| \sum_{i=0}^{N_{\mathrm{FFT}}-1} z_n(t) e^{-\frac{j2\pi it}{N_{\mathrm{FFT}}}} \right|^2 \tag{12}$$

where N_{FFT} is the Fast Fourier Transform (FFT) length and $\mathbf{z} = \mathbf{Vx}$ is $N \times 1$ vector of precoded symbols. The load-dependent power consumption of the RF module is mostly caused by the PA and thus we approximate it using the PA power consumption model for base stations. For the b-way Doherty PA, where b is a positive integer, the power consumption is expressed as [31]

$$P_{\mathrm{PA}}(P_{\mathrm{in}}) = \frac{4P_{\mathrm{out}}^{\max}}{b\pi} \begin{cases} \sqrt{\frac{P_{\mathrm{in}}}{P_{\mathrm{in}}^{\max}}}, & 0 \leq P_{\mathrm{in}} < \frac{P_{\mathrm{in}}^{\max}}{b^2} \\ (b+1)\sqrt{\frac{P_{\mathrm{in}}}{P_{\mathrm{in}}^{\max}}} - 1, & \frac{P_{\mathrm{in}}^{\max}}{b^2} \leq P_{\mathrm{in}} < P_{\mathrm{in}}^{\max} \end{cases} \tag{13}$$

where $P_{\mathrm{in}}^{\max} = \rho E[P_{\mathrm{in}}]$ is the peak RF input power and $P_{\mathrm{out}}^{\max} = G P_{\mathrm{in}}^{\max}$ is the corresponding peak output power of the PA. The parameters ρ and G are the input power back-off and the transmitted power gain, respectively. We use a soft limiting model for the PA, i.e. it is assumed to be linear until $P_{\mathrm{out}}^{\max}$ at which the RF input powers greater than $P_{\mathrm{in}}^{\max}$ are clipped due to saturation. By choosing large enough input power back-off (IBO), we can ignore the effect of clipping. The efficiency of the PA is given by $\eta = P_{\mathrm{out}}/P_{\mathrm{PA}}$ where $P_{\mathrm{out}} = G P_{\mathrm{in}}$ is the transmitted power.

3 Dynamic point selection and scheduling

The objective in this study is to improve the average energy efficiency in the distributed antenna system described in Section 2 such that the cell edge spectral efficiency is not degraded. The average energy efficiency ϵ_c for sector c is defined as

$$\epsilon_c = \frac{\sum_{i=1}^{N_f} B_{c,i}}{\sum_{i=1}^{N_f} \sum_{j=1}^{N_s} P_{c,i,j} T_s} \tag{14}$$

where N_f is the number of considered subframes, $B_{c,i}$ is the number of received DL physical layer data bits in subframe i within sector c, N_s is the number of samples in a subframe, $P_{c,i,j}$ is the consumed power for sample j according to (11), and T_s is the sampling interval. The cell edge spectral efficiency is defined as 5 % point of the cumulative distribution function (cdf) of the user throughput divided by the channel bandwidth [3]. In this study,

the user throughput is defined as the number received physical layer bits for the user in a second.

As a solution to this problem, we propose a DPS method that combines static inter-cell coordinated TP scheduling with the enhanced DTX. In addition, we also present a non-coordinated DPS and TP scheduling method for scenarios in which the inter-cell agreement is not possible.

3.1 Static TP activity agreement

In our proposed method, the static inter-cell coordinated TP scheduling reduces the inter-cell interference and enhanced DTX combined with switching on/off RF chains reduces the power consumption. When the enhanced DTX is in use, it is possible to put all but the active TP into short sleep modes. In order not to compromise the cell coverage, the sleep modes are not allowed on subframes 0 and 5 when the synchronization and broadcast signals are transmitted. The inter-cell coordinated scheduling is based on the static agreement between cells on which TP is active during the given subframe. When each sector has the same number of TPs (as assumed in Section 2), it is convenient to set the agreement such that the TPs with the same index are active at the same time in each sector. This is illustrated in Fig. 4 where $N = 2$, $\Gamma = 3$, and UEs A and B are served by the center cell. At subframes when UE A is served, only the RRHs are transmitting and the RF chains of eNBs are switched off. Similarly at subframes when UE B is served, only the eNBs are transmitting and RF chains of RRHs are switched off. This effectively halves the number of dominant interferers when compared to the situation in Fig. 2 and reduces the power consumption. The UEs who have selected different TPs by the DPS procedure are always scheduled for different subframes.

Let $\boldsymbol{\nu} \in \{1, \ldots, N\}$ be the $U \times 1$ static indicator vector of the active TP for all sectors in the network where U is the DPS interval, i.e. the number of subframes during which the selected TP for a UE is not changed. This effectively means that the same TP index is active in all sectors and the interference is at the same level for those subframes whose ν_u are equal. In order to perform DPS, information about the channel quality corresponding to each TP-UE pair is needed at the base station. When $N \leq 3$, it is possible to configure the UE to report CQI using N different single antenna CSI processes [22] such that CSI process n corresponds to the scenario when TP n is active. When $N > 3$, the CQI for the 3 best TPs can be maintained using the CoMP resource management procedure described in [15]. UEs are divided into $\mathcal{X}_n, n = 1, \ldots, N$ where $\mathcal{X}_n$ is the set of UEs whose wideband CQI is highest when served by TP n. Let $\boldsymbol{\omega}^{(k)}$ be a $N \times 1$ vector of wideband CQI values for UE k. The proposed DPS and scheduling algorithm can be presented as follows

1. Configure each UE to report CQI using N different CSI processes.
2. Set the TP activity indicators $\boldsymbol{\nu}$ according to the network configuration.
3. Initialize sets $\mathcal{X}_n = \{\emptyset\}$ for $n = 1, \ldots, N$. Set the subframe index $u = 0$.
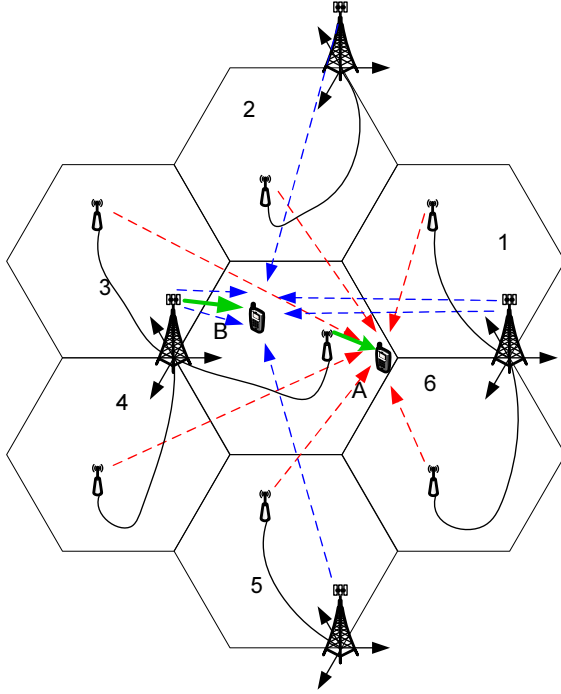
Fig. 4 Dominant interferers when the proposed method is used in the 3 sector deployment. Red and blue dashed arrows depict the interfering signal from the dominant interferers to UE A and B, respectively

4. Fill the UE sets: $\mathcal{X}_n = \{k | n = \arg\max_n \omega_n^{(k)}, k \in \{1, \ldots, K\} \}$ for $n = 1, \ldots, N$.

5. Set $n = \nu_u$. Schedule the UEs in $\mathcal{X}_n$ to be transmitted from TP n in this subframe.

6. Set $u = u + 1$. If $u < U$, go to Step 5. Else go to Step 3.

The above algorithm has no mechanism to improve the spectral efficiency for cell edge UEs. The average spectral efficiency can be traded off for cell edge spectral efficiency by restricting the access to frequency-selective scheduling only for those UEs whose number of scheduled data bits $Y^{(k)}$ is below the target $\hat{Y}$. This obviously violates the resource-fair principle since the UEs with low CQI get more resource blocks during the DPS interval. When we omit the configuration steps 1-2 from the above algorithm, the modified cell edge boosted DPS and scheduling algorithm becomes

3. Initialize sets $\mathcal{X}_n = \{\emptyset\}$ for $n = 1, \ldots, N$. Set the subframe index $u = 0$. Set $Y^{(k)} = 0$ for $k = 1, \ldots, K$

4. Set $n = \nu_u$.

5. Fill the UE set: $\mathcal{X}_n = \{k | n = \arg\max_n \omega_n^{(k)}, Y^{(k)} < \hat{Y}, k \in \{1, \ldots, K\} \}$.

6. If $|\mathcal{X}_n| = 0$, refill the UE set: $\mathcal{X}_n = \{k | n = \arg\max_n \omega_n^{(k)}, k \in \{1, \ldots, K\}\ \}$.

7. Schedule the UEs in $\mathcal{X}_n$ to be transmitted from TP n in this subframe. Update $Y^{(k)}$ for UEs in $\mathcal{X}_n$.

8. Set $u = u + 1$. If $u < U$, go to Step 4. Else go to Step 3.

It is not straightforward to select the TP activity vector $\boldsymbol{\nu}$ such that the average energy efficiency is maximized under the cell edge spectral efficiency constraint. From the power consumption point of view, it makes sense to put the RF circuits of the high-power eNB into short sleep modes as often as possible. On the other hand, UEs close to the eNB typically have the highest CQI. Thus from the sum spectral efficiency point of view, eNBs should be transmitting as often as possible. A good approach is to set the fraction of time, when TP n is active, to the same level as the expected fraction of UEs that have selected TP n by the DPS procedure. This can be calculated offline when the probability distributions of UE locations and the channel coefficients are known. Another design question is whether a TP should have its active subframes sequentially or distributed over the duration of the DPS interval. In case of delay-sensitive traffic, it is better to have the active subframes distributed to avoid long periods without transmission for a UE. On the other hand from the RF equipment point of view, it is not easy to efficiently implement very short sleep modes and thus the sequential ordering of active subframes is preferred. The duration of the DPS interval U should be set according to the periodicity of the wideband CQI reporting. In scenarios with mostly pedestrian UEs, U can be relatively long because the best TP for a UE is expected to be the same for hundreds of subframes.

The main benefit of our method is that it is fully compatible with the LTE-A standard. On the other hand, the basic idea of the proposed method can be applied to any distributed antenna system. Inter-cell coordination is based on a static agreement that can be exchanged during network configuration. Thus unlike in inter-cell CoMP methods [32], there is no need for runtime backhaul signalling or data exchange. The method works in any traffic scenarios but the best performance is achieved under medium to heavy traffic loads. Under low load, some TPs may be active even if they do not have any UEs to serve. This obviously reduces the energy efficiency.

3.2 Non-coordinated active TP selection

In some cases inter-cell agreement on the TP activity is not possible due to e.g. having different operators at neighbouring cells. For these cases, we present an algorithm for TP selection that requires no inter-cell coordination. Unlike in the methods presented in Section 3.1, the number of subframes for a TP can be dynamically adapted for each DPS interval. In the presented method, a subframe is allocated for the TP that is transmitting to the UE with the lowest throughput during the DPS interval. Let $\boldsymbol{z} \in \{1, \ldots, N\}$ be a $K \times 1$ vector where z_k indicates the TP selected by the DPS procedure of UE k. The proposed non-coordinated TP selection algorithm can be presented as follows

1. Configure each UE to report CQI using N different CSI processes.
2. Initialize sets $\mathcal{X}_n = \{\emptyset\}$ for $n = 1, \ldots, N$. Set the subframe index $u = 0$. Set the UE index $k = 1$.
3. Find the best TP for UE k: $n = \arg\max_n \omega_n^{(k)}$.
4. Include UE k into $\mathcal{X}_n$: $\mathcal{X}_n = \mathcal{X}_n \cup \{k\}$. Set $z_k = n$.
5. Set $k = k + 1$. If $k \leq K$, go to Step 3.
6. Find the UE with the minimum number of scheduled bits: $k_{\min} = \arg\min_k Y^{(k)}$.
7. Set $n = z_{k_{\min}}$. Schedule the UEs in $\mathcal{X}_n$ to be transmitted from TP n in this subframe. Update $Y^{(k)}$ for UEs in $\mathcal{X}_n$.
8. Set $u = u + 1$. If $u < U$, go to Step 6. Else go to Step 2.

Compared to the inter-cell coordinated methods presented in Section 3.1, the above algorithm does not waste any resources in low load situations. If a TP is not selected by any UE, no subframes are reserved for it for the duration of the DPS interval. However because there is no inter-cell coordination on the TP activity, the level of interference varies randomly and occasional severe interference on some UEs can have a significant effect on the performance. Strong variation of interference levels also causes challenges to the SINR estimation process of the UEs. According to the LTE standard [23], UEs have to report such CQI that guarantees block error rate (BLER) less than 10 %. A conservative strategy, which always achieves the BLER target, is to use the highest interference levels from the previous U subframes when calculating the CQI to be reported. With static TP activity agreement methods, severe inter-cell interference can be avoided, especially when the placement of remote antennas is optimized according to Section 4.

4 Remote antenna placement

Our goal is to place the remote antennas such that the cell edge spectral efficiency is improved compared to the random placement. In order to reduce the complexity of the problem, we restrict the relative remote antenna locations to be the same in each sector with respect to the sector boresight. In order to be independent of the receiver processing, the cell edge normalized capacity is used as the placement criterion. Let the instantaneous normalized capacity of DPS for UE k be defined as

$$C^{(k)} = \log_2\left(1 + \max\left\{\hat{\gamma}^{(k,1)}, \ldots, \hat{\gamma}^{(k,N)}\right\}\right) \tag{15}$$

where $\hat{\gamma}^{(k,n)}$ is the received SINR given that the nth TP is used for transmission. Since the same TP is active in all sectors at the same time, $\hat{\gamma}^{(k,n)}$ simplifies to

$$\hat{\gamma}^{(k,n)} = \frac{\left|\mathbf{h}_n^{(k)}\right|^2}{\sum_{i=1}^{I}\left|\mathbf{h}_n^{(k,i)}\right|^2 + \sigma^2}. \tag{16}$$

It can be seen from (2) that each channel coefficient $\mathbf{h}_n^{(k)}$ is a function of $3+M$ random variables: $d_n^{(k)}, \theta_n^{(k)}, S_n^{(k)}, F_{1,n}^{(k)}, \ldots F_{M,n}^{(k)}$. Thus the exact analysis of the cdf of $C^{(k)}$ is tedious and the cdf can be approximated by Monte Carlo simulations. The exhaustive search for the remote antenna location that maximizes the 5 % point of the cdf of $C^{(k)}$ is computationally feasible when $N = 2$.

The effect of the remote antenna placement optimization is illustrated in Fig. 5 and Fig. 6 where the conditional average normalized capacity given the fixed shadowing and multipath fading as a function of the UE location are shown for the sector center placement and the optimized placement, respectively when $N = 2$ and $\Gamma = 6$. When drawing Fig. 5 and Fig. 6, we have assumed that $S_n^{(k)} = E[S], \forall n$ and $F_{m,n}^{(k)} = E[F], \forall m, n$. It is also assumed that the minimum eNB-UE distance is 35 m and the minimum RRH-UE distance is 10 m. This explains the zero-capacity white circles at the eNB and RRH locations. It can be seen from Fig. 5 and Fig. 6 that the optimized RRH placement clearly reduces the dark blue area, i.e. the area where the capacity is likely to be poor.

5 Numerical results

Due to the complexity of the system, the performance of the proposed method is evaluated by simulations. The simulator is built upon the University of Vienna DL LTE Link Level Simulator [26] that has been extended to support the sectored and distributed layout, the channel model given in (2), and the inter-cell interference aware post-processing SINR calculation given in (6). In this work, the main benefit from using the Vienna LTE link level simulator is that it accurately models the output complex baseband samples from the eNB physical layer to RF processing. This enables the modelling of the PA consumed power according to (13).

Unless otherwise stated, the numerical parameter values shown in Table 2 are used in simulations. Most of the parameter values are selected according to the recommendations in [16]. Note that the transmitted power gain G equals the per-antenna average value for the transmitted power in the distributed scenario and the sum of average per-antenna transmitted power values in the localized scenario. Static TP activity indicator vector is set to $\boldsymbol{\nu} = [1\ 2\ 1\ 2\ 1\ 2\ 1\ 2\ 1\ 1]^T$. The division of reserving 60 % of the subframes for eNB transmission and 40 % for RRH transmission was selected based on our offline simulations because it achieved better cell edge spectral efficiency than other divisions. The target number of scheduled data bits $\hat{Y}$ for the cell edge boosted algorithm is set to equal the simulated cell edge spectral efficiency of the localized MIMO multiplied by the subframe duration and by the channel bandwidth. When non-coordinated active TP selection is used, it is assumed that UEs report the CQI corresponding to the lowest SINR during the DPS interval. As discussed in Section 3.2, this guarantees that the BLER target is always fulfilled.
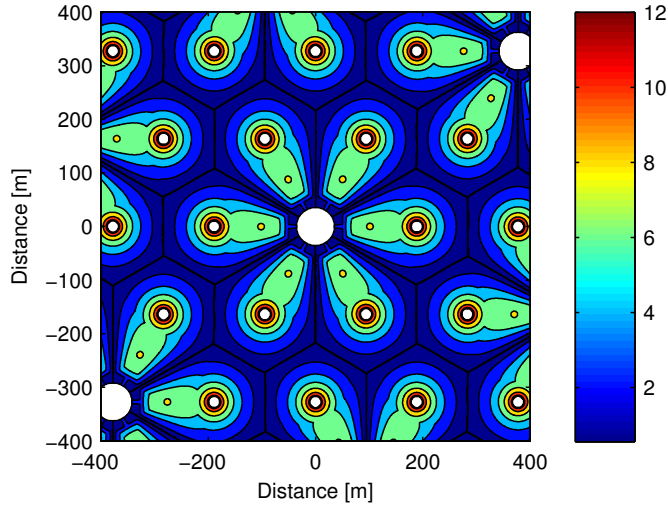
Fig. 5 Conditional average normalized capacity [bit/s/Hz] given the fixed shadowing and multipath fading as a function of the UE location for the center RRH placement
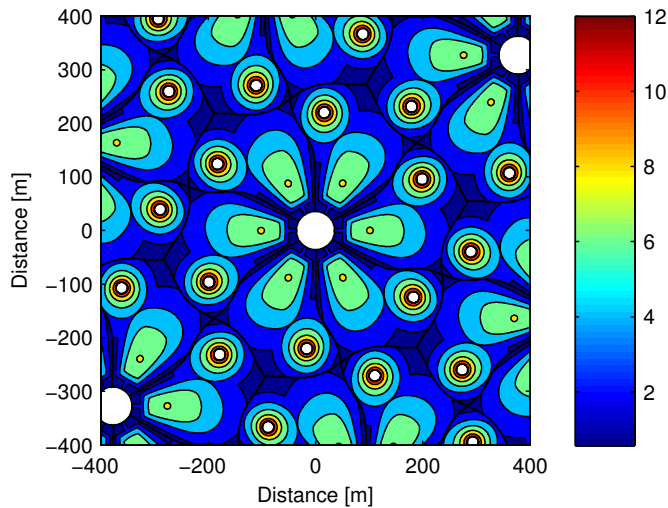

Fig. 6 Conditional average normalized capacity [bit/s/Hz] given the fixed shadowing and multipath fading as a function of the UE location for the optimized RRH placement

For the remainder of the paper, the identifier MIMO is referring to the localized scenario, DMIMO to the distributed scenario with no DPS, and DPS-Bx and DPS-Ax to the DPS scenarios with and without cell edge boosting scheduling, respectively. The identifier DPS-Cx refers to the DPS method with non-cooperative active TP selection between neighbouring cells. The last letter in the DPS identifier indicates whether the RRH location is random (R) or

Table 2 Parameter values for simulations

Parameter	Value
Number of base station antennas per sector, N	2
Number of UE antennas, M	2
Noise variance, σ^2	$3.16 \cdot 10^{-13}$
Transmitted power gain, G	39.81, eNB
	5.01, RRH
Sum of antenna gains, G_{ant}	17 dB, 3-sector eNB
	20 dB, 6-sector eNB
	5 dB, RRH
Shadowing standard deviation, σ_S	6 dB, eNB
	4 dB, RRH
Horizontal 3 dB beamwidth, $\theta_{3\mathrm{dB}}$	70°, 3-sector
	35°, 6-sector
Horizontal maximum attenuation, A_m	25 dB, 3-sector
	28 dB, 6-sector
Height difference between transmitting and	23.5 m, eNB
receiving antennas, h	8.5 m, RRH
Tilt angle, ϕ_{tilt}	12°
Vertical 3 dB beamwidth, $\phi_{3\mathrm{dB}}$	10°
Vertical maximum attenuation, $A_{m,v}$	20 dB
Constant path loss, κ	19.57 dB, eNB
	30.53 dB, RRH
Path loss exponent, α	3.91, eNB
	3.67, RRH
Digital baseband power consumption, P_P	23.33 W
Sleep mode coefficient, a	0.1
Static RF power consumption, P_R	75 W, eNB
	37.5 W, RRH
FFT length, N_{FFT}	1024
Doherty PA order, b	3
Input power back-off, ρ	15.85
Number of simulated subframes, N_f	100000
Number of samples in subframe, N_s	15360
Sampling interval, T_s	65.10 ns
Channel bandwidth	10 MHz
DPS interval, U	10
Minimum eNB-RRH distance	75 m
Minimum eNB-UE distance	35 m
Minimum RRH-UE distance	10 m

optimized (O). For example, the identifier DPS-BO refers to the scenario with cell edge boosting and the optimized RRH location.

5.1 Cell edge spectral efficiency

The cell edge spectral efficiency as a function of the number of UEs is shown in Fig. 7 and Fig. 8 for 3 and 6 sectors, respectively. It can be seen that by simply applying closed-loop spatial multiplexing in the distributed scenario, the cell edge spectral efficiency is decreased when compared to the localized scenario. When there is no coordination over the placement of the RRH and

over the inter-cell interference, the potential benefit from macro-diversity is cancelled out by the increased inter-cell interference. When both the RRH placement and the inter-cell interference are coordinated, as in the DPS-AO case, approximately the same cell edge spectral efficiency can be reached as in the localized scenario. The best cell edge spectral efficiency is reached by the cell edge boosting scheduling that prioritizes the UEs with bad CQI by allocating them more PRB resources. In the DPS-Cx cases, the level of inter-cell interference varies randomly between subframes. Occasional severe inter-cell interference causes the cell edge spectral efficiency to be lower than in the localized reference scenario. The poor cell edge performance of DPS-Cx methods is also partially explained by the conservative CQI reporting procedure of the UEs. The cell edge spectral efficiency levels in the 6-sector layout are only slightly better than in the 3-sector layout. Even though the received signal strength is on the average at a higher level in the 6-sector layout, the denser deployment also increases the interference level cancelling out most of the gain. Based on the results in Fig. 7 and Fig. 8, it can be concluded that the cell edge spectral efficiency is not degraded compared to the localized case in cases DPS-AO when $K \geq 6$, DPS-BR, and DPS-BO. The results are also very well in line with the IMT-A cell edge spectral efficiency requirement, which is 0.06 bit/s/Hz for 10 UEs in the base coverage urban scenario [3]. However, the IMT-A target value is not directly applicable to our work because it is defined for 4×2 MIMO setting using the bits in Layer 3 service data units.

5.2 Average energy efficiency

The average energy efficiency as a function of the number of UEs is shown in Figs. 9 and 10 for 3 and 6 sectors, respectively. It is clearly seen that our proposed method provides a significant increase in the average energy efficiency with (DPS-Bx) and without (DPS-Ax) cell edge boosting. The energy efficiency gain is mainly caused by the reduced power consumption from switching off the RF chains of inactive TPs. As mentioned in Section 3, cell edge boosting trades the cell spectral efficiency off for the cell edge spectral efficiency. This is visible also in Figs. 9 and 10 in which the average energy efficiency of DPS-BO is lower than that of DPS-AO. The DPS method with non-cooperative active TP selection between neighbouring cells (DPS-Cx) achieves the best average energy efficiency for a single UE. This can be explained by the adaptive number of subframes allocated for a TP. Thus unlike with DPS-Ax and DPS-Bx methods, no resources are wasted in situations with low number of UEs. The energy efficiency gain from 6 sectors is only marginal because according to the used power consumption model, the base station power consumption increases linearly with the number of sectors.

   Since the energy efficiency improvement of our proposed method comes mainly from switching off inactive RF chains, the amount of gain is highly dependent on the parameters of the power consumption model. The best energy efficiency is reached when the load-independent RF power consumption is
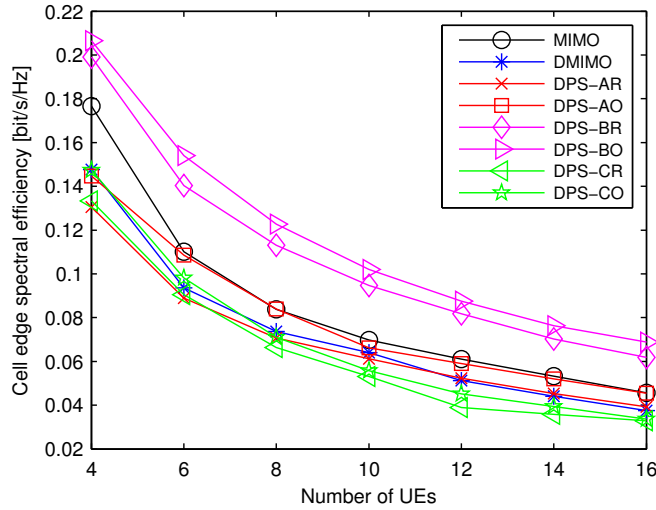
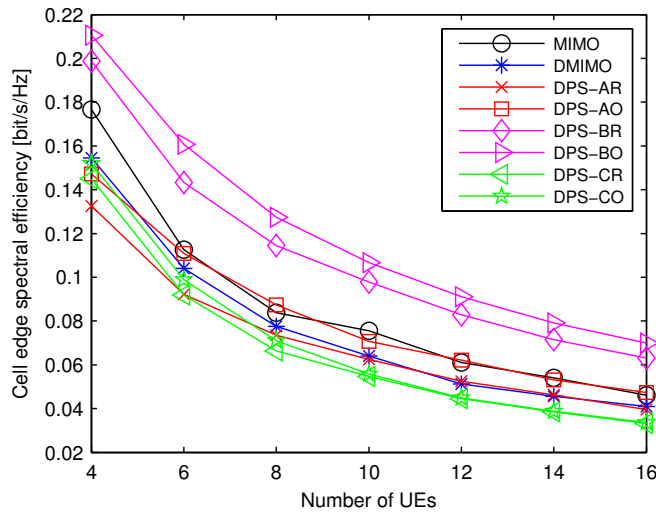**Fig. 7** Cell edge spectral efficiency as a function of the number of UEs in the 3-sector layout

Fig. 8 Cell edge spectral efficiency as a function of the number of UEs in the 6-sector layout

high in the active mode and low in the sleep mode. The values for parameters P_P and P_R in Table 2 have been selected based on the input from partners in the OPERA-Net2 project [33]. Using those values, the load-independent power consumption of a single eNB RF chain $P_{R,\mathrm{eNB}}$ contributes to 43.3 % of the total load-independent power consumption $P_F = P_P + \sum_{n=1}^{N} P_{R,\mathrm{eNB}}$ in the localized 2×2 MIMO reference scenario. Let the energy efficiency gain δ be defined as $\delta = (\epsilon_c/\epsilon_{c,\mathrm{MIMO}} - 1) \cdot 100\%$ where $\epsilon_{c,\mathrm{MIMO}}$ is the average energy efficiency in the localized 2×2 MIMO reference scenario. The energy efficiency gain
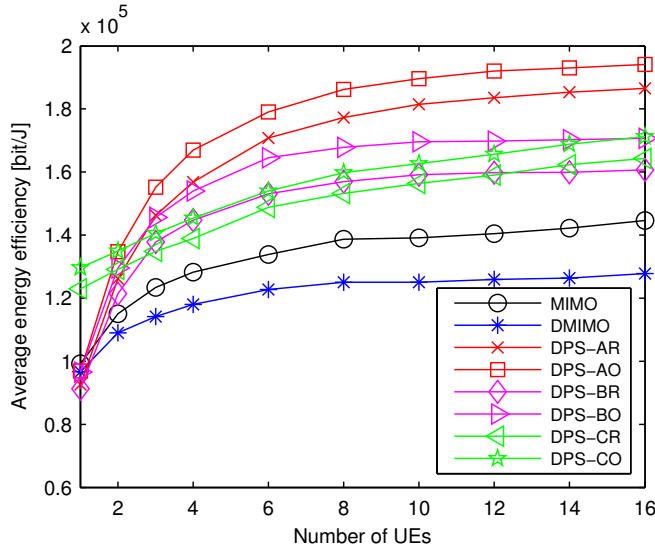
Fig. 9 Average energy efficiency as a function of the number of UEs in the 3-sector layout
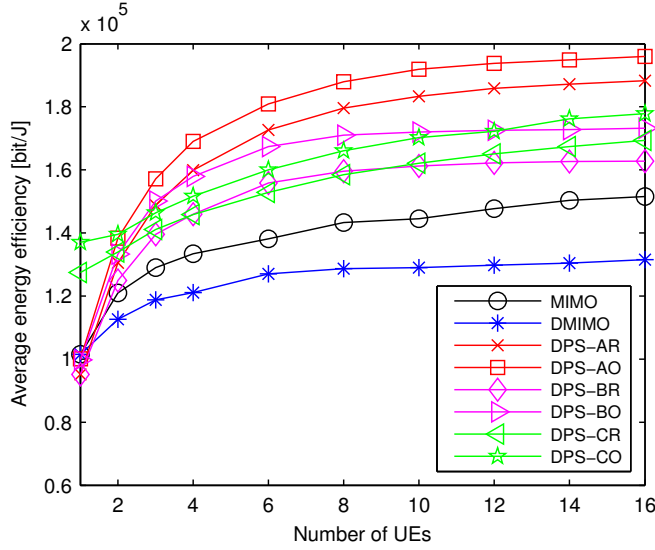

Fig. 10 Average energy efficiency as a function of the number of UEs in the 6-sector layout

as a function of normalized load-independent RF power $P_{R,\text{eNB}}/P_F$ and sleep mode coefficient a is shown in Fig. 11 for the DPS-AO method with 10 UEs in the 3-sector layout. For Fig. 11, it is assumed that the load-independent RRH RF power is $P_{R,\text{RRH}} = P_{R,\text{eNB}}/2$ and the total power consumption $P_{c,\text{DPS}}$ is kept constant. The white area indicates when the proposed DPS-AO method achieves negative energy efficiency gain and should not be used. The x marker
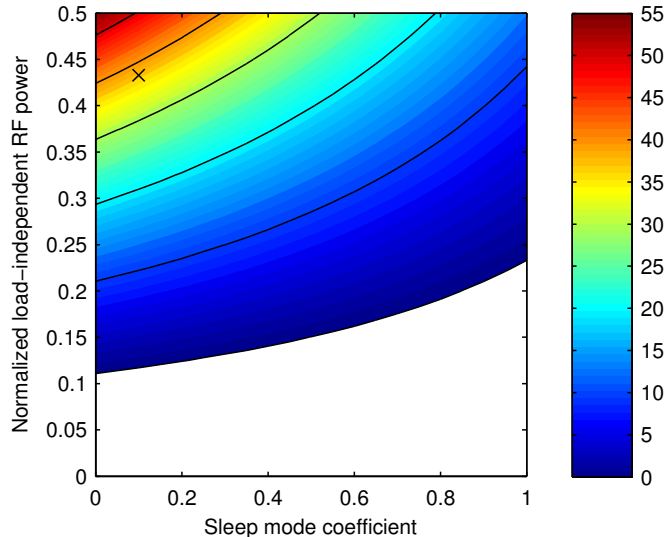
Fig. 11 Energy efficiency gain in % as a function of normalized load-independent RF power $P_{R,\mathrm{eNB}}/P_F$ and sleep mode coefficient a for the DPS-AO method with 10 UEs in the 3-sector layout

at 35 % contour indicates the energy efficiency gain using the parameter values from Table 2.

Based on Fig. 11, we can conclude that when the normalized load-independent RF power exceeds a certain limit, 22 % in our example case, the DPS-AO method brings always energy efficiency gain even when RF chain sleeping cannot be implemented, i.e. $a = 1$. On the other hand when the normalized load-independent RF power is below a certain limit, 11 % in our example, the DPS-AO method does not bring energy efficiency gain. However, this limit is usually exceeded in macro base station power consumption models. For example, the normalized load-independent RF power is 15.3 % in [34] and 33.3 % in [35]. The same kind of limits can be found for any number of UEs and also for the 6-sector layout.

6 Conclusions

In this paper, we have studied how to improve the energy efficiency under full load in the intra-cell CoMP scenario 4 such that the cell edge spectral efficiency is not degraded. A novel DPS and time domain UE scheduling method has been presented as a solution to this problem. The key idea of the proposed method is to transmit from only one antenna of the cell during a subframe and switch the unused RF chains off for power consumption reduction. In addition, the inter-cell interference is reduced by statically agreeing between cells which TPs are active at a given subframe.

According to the numerical results from performance simulations, our proposed method can reach significant improvement compared to localized and distributed SU-MIMO in energy efficiency without cell edge spectral efficiency degradation. The energy efficiency is improved by 35 % when 10 UEs are served by the sector. It is shown that the cell edge spectral efficiency of closed-loop spatial multiplexing in the distributed scenario with randomly located RRH is worse than in the localized scenario. The cell edge spectral efficiency in the distributed scenario can be improved by inter-cell interference coordination and optimization of the RRH locations. We have also studied the effect of the power consumption modelling to the performance of our method. When the proportion of the load-independent RF power consumption to the total load-independent power consumption exceeds a certain limit, which is 22 % in the case of 10 UEs in the 3-sector layout, the proposed method brings always energy efficiency gain even when RF chain micro sleeping cannot be implemented. In general, the proposed method performs well when the load-independent RF power consumption is high in the active mode and low in the sleep mode.

The main benefit of our method is that it is fully compatible with the LTE-A standard. The coordination between different cells is based on a static agreement and thus there is no need for low latency or high throughput backhaul. Unlike most of the proposed improvements to LTE-A energy efficiency, our method is applicable also under heavy load. The basic idea in this paper can be applied to any system based on distributed antennas.

The numerical results in this paper have been restricted to the case where there is only a single RRH per sector. As a further work, the performance could be evaluated also with the higher number of remote antennas. It would be interesting to evaluate if the proposed method could be used as a low complexity alternative to MU-MIMO methods in distributed antenna systems. Another direction for further work would be to evaluate the performance of the proposed method analytically using a simplified system model.

References

1. Chen, L., Wang, W., Anpalagan, A., Vasilakos, A.V., Illanko, K., Wang, H., et al. (2013). Green cooperative cognitive communication and networking: A new paradigm for wireless networks. *Mobile Netw. Appl.*, 18(4), 524–534.
2. Alsharif, M.H., Nordin, R., & Ismail, M. (2014). Classification, recent advances and research challenges in energy efficient cellular networks. *Wireless Pers. Commun.*, 77(2), 1249–1269.
3. ITU-R Report M.2134, (2008). *Requirements related to technical performance for IMT-Advanced radio interface(s)*.

4. Ghosh, A., Ratasuk, R., Mondal, B., Mangalvedhe, N., & Thomas, T. (2010). LTE-Advanced: Next-generation wireless broadband technology. *IEEE Wireless Commun. Mag.*, 17(3), 10–22.
5. Chen, T., Yang, Y., Zhang, H., Kim, H., & Horneman, K. (2011). Network energy saving technologies for green wireless access networks. *IEEE Wireless Commun. Mag.*, 18(5), 30–38.
6. Frenger, P., Moberg, P., Malmodin, J., Jading, Y., & Gódor, I. (2011). Reducing energy consumption in LTE with cell DTX. in *Proc. IEEE VTC Spring*. Budapest, Hungary.
7. Wang, R., Thompson, J., Haas, H., & Grant, P. (2011). Sleep mode design for green base stations. *IET Communications*, 5(18), 2606–2616.
8. Goldsmith, A., Jafar, S.A., Jindal, N., & Vishwanath, S. (2003). Capacity limits of MIMO channels. *IEEE J. Sel. Areas Commun.*, 21(5), 684–702.
9. Kakitani, M.T., Brante, G., Souza, R.D., & Imran, M.A. (2013). Energy efficiency of transmit diversity systems under a realistic power consumption model. *IEEE Commun. Lett.*, 17(1), 119–122.
10. Cui, S., Goldsmith, A.J., & Bahai, A. (2004). Energy-efficiency of MIMO and cooperative MIMO techniques in sensor networks. *IEEE J. Sel. Areas Commun.*, 22(6), 1089–1098.
11. Héliot, F., Imran, M.A., & Tafazolli, R. (2012). On the energy efficiency-spectral efficiency trade-off over the MIMO Rayleigh fading channel. *IEEE Trans. Commun.*, 60(5), 1345–1356.
12. Onireti, O., Heliot, F., & Imran, M.A. (2013). On the energy efficiency-spectral efficiency trade-off of distributed MIMO systems. *IEEE Trans. Commun.*, 61(9), 3741–3753.
13. Xu, J. & Qiu, L. (2013). Energy efficiency optimization for MIMO broadcast channels. *IEEE Trans. Wireless Commun.*, 12(2), 690–701.
14. Irmer, R., Droste, H., Marsch, P., Grieger, M., Fettweis, G., Brueck, S., et al. (2011). Coordinated multipoint: Concepts, performance, and field trial results. *IEEE Commun. Mag.*, 49(2), 102–111.
15. Lee, J., Kim, Y., Lee, H., Ng, B.L., Mazzarese, D., Liu, J., et al. (2012). Coordinated multipoint transmission and reception in LTE-Advanced systems. *IEEE Commun. Mag.*, 50(11), 44–50.
16. 3GPP Technical Report TR 36.819, (2011). *Coordinated multi-point operation for LTE physical layer aspects*, Rev. 11.1.0.
17. Holtkamp, H., Auer, G., Bazzi, S., & Haas, H. (2014). Minimizing base station power consumption. *IEEE J. Sel. Areas Commun.*, 32(2), 297–306.
18. Abdallah, K., Cerutti, I., & Castoldi, P. (2012). Energy-efficient coordinated sleep of LTE cells. in *Proc. IEEE ICC*. Ottawa, Canada.
19. ITU-R Report M.2135, (2008). *Guidelines for evaluation of radio interface technologies for IMT-Advanced*.
20. Chhedda, A. & Bassirat, F. (1999). Enhanced cellular layout for CDMA networks having six-sectored cells. *U.S. Patent* 5 960 349.
21. Sheikh, M.U. & Lempiäinen, J. (2013). A flower tessellation for simulation purpose of cellular network with 12-sector sites. *IEEE Wireless Commun. Lett.*, 2(3), 279–282.
22. 3GPP Technical Specification TS 36.211, (2013). *Physical channels and modulation*, Rev. 11.5.0.
23. 3GPP Technical Specification TS 36.213, (2013). *Physical layer procedures*, Rev. 11.5.0.
24. Schwarz, S., Mehlführer, C., & Rupp, M. (2010). Calculation of the spatial preprocessing and link adaptation feedback for 3GPP UMTS/LTE. in *Proc. WiAD Conf.* London,UK.
25. Nam, Y.H., Akimoto, Y., Kim, Y., il Lee, M., Bhattad, K., & Ekpenyong, A. (2012). Evolution of the reference signals for LTE-Advanced systems. *IEEE Commun. Mag.*, 50(2), 132–138.
26. *Vienna LTE simulators: Link level simulator documentation v1.7r1089*, (2011). Institute of Telecommunications, Vienna University of Technology, Vienna, Austria.
27. Ikuno, J.C., Wrulich, M., & Rupp, M. (2010). System level simulation of LTE networks. in *Proc. IEEE VTC Spring*. Taipei, Taiwan.
28. Berggren, F. & Jäntti, R. (2003). Multiuser scheduling over Rayleigh fading channels. in *Proc. IEEE GLOBECOM*. San Francisco, CA.
29. ETSI TR 103.117, (2012). *Principles for mobile network level energy efficiency*, Rev. 1.1.1.

30. Varma, V.S., Elayoubi, S.E., Debbah, M., & Lasaulce, S. (2013). On the energy efficiency of virtual MIMO systems. in *Proc. IEEE PIMRC*. London, UK.

31. Joung, J., Ho, C.K., & Sun, S. (2014). Spectral efficiency and energy efficiency of OFDM systems: Impact of power amplifiers and countermeasures. *IEEE J. Sel. Areas Commun.*, 32(2), 208–220.

32. Li, G.Y., Niu, J., Lee, D., Fan, J., & Fu, Y. (2014). Multi-cell coordinated scheduling and MIMO in LTE. *IEEE Commun. Surveys Tuts.*, 16(2), 761–775.

33. Lasanen, M., Aubree, M., Cassan, C., Conte, A., David, J., Elayoubi, S.E., et al. (2013). Environmental friendly mobile radio networks: Approaches of the European OPERA-Net 2 project. in *Proc. ICT*. Casablanca, Morocco.

34. Holtkamp, H., Auer, G., Giannini, V., & Haas, H. (2013). A parameterized base station power model. *IEEE Commun. Lett.*, 17(11), 2033–2035.

35. Deruyck, M., Joseph, W., Lannoo, B., Colle, D., & Martens, L. (2013). Designing energy-efficient wireless access networks: LTE and LTE-Advanced. *IEEE Internet Comput.*, 17(5), 39–45.